JOURNAL OF Materials CHEMISTRY

Surface contact studies of NaCl and TiO_2: molecular dynamics simulation studies

Chin W. Yong,*[a] William Smith[a] and Kevin Kendall[b]

[a]*CCLRC, Daresbury Laboratory, Daresbury, Warrington, UK WA4 4AD. E-mail: c.w.yong@dl.ac.uk*
[b]*School of Chemical Engineering, The University of Birmingham, Edgbaston, Birmingham, UK B15 2TT*

Received 12th March 2002, Accepted 27th June 2002
First published as an Advance Article on the web 6th August 2002

A series of molecular dynamics simulations have been performed at 300 K to investigate the differences between commensurate surface contact interactions of NaCl and TiO_2. The contact studies were carried out between two bodies of identical material which consisted of blocks of NaCl probes (with cross-section $n \times n$, where $n = 2$, 4, 6, 8 and 10 atoms) and blocks of TiO_2 probes (with cross-section $2 \times m$, where $m = 4$, 5, 6, 7 and 8 unit cells) with NaCl (001) and TiO_2 (110) surface slabs, respectively. By studying the vertical force as a function of distance between the probes and surfaces and the corresponding atomic configurations, mechanistic descriptions of the probes' contact with the surfaces and subsequent withdrawal have been obtained. We have observed both a characteristic instability 'jump' involving large atomic displacements and an increase in attractive force in both materials. However, the nature of the jump processes differ in that a more elaborate atomic reorganisation occurs in TiO_2 during the jump process, whereas it is essentially a straightforward, commensurate contact for the NaCl system. In addition, the NaCl probes can be withdrawn completely from the surface with no permanent structural change to the probe but with an associated hysteresis at the jump region. Conversely, withdrawal in the TiO_2 systems depends on the extent of compression on the probe. At sufficiently high compression, a probe may collapse and subsequently fuse at the contact junction. The withdrawal of the TiO_2 probes also shows complex behaviour, whereby the initial creation of a defect hole leads to the formation and subsequent elongation of a necking structure at the lower part of the probe.

Introduction

The study of two surfaces in close contact is important for the understanding of adhesion and friction, which occur whenever two moving bodies come into contact. The frictional force acts in a direction parallel but opposite to the motion of the bodies, whereas adhesion is the normal force. The macroscopic nature of friction has been extensively studied since as far back as three hundred years ago[1] and it has been known for quite some time that the adhesive forces between the bodies in contact play an important role in the overall frictional resistance. However, the atomic mechanisms that underlie macroscopically observed adhesion and frictional phenomena are still poorly understood. The coefficient of friction, which is introduced to describe contact mechanics in many theoretical treatments and computer simulations of granular materials,[2–4] is at best phenomenologically derived and without sound scientific justification at the atomistic level.

On the experimental front, recent surface-sensitive techniques such as atomic force microscopy[5–8] have begun to shed light on micro-contact responses between an atomic scale tip-like body and a surface. Such studies are particularly relevant to friction, since real macroscopic body contacts usually occur in a number of discrete areas, whereby microscopic raised projections of one body make contact with the surface of the other. In reality, contact interactions are very complex and difficult to characterise. This is because results are inevitably complicated by undesirable factors that are present in experiments. For example, surface defects and contaminants such as adsorbed layers of hydrocarbons or water molecules. These factors, together with the underlying surface molecular interactions, give rise to the overall observed frictional phenomenon. Clearly, it is desirable to isolate and investigate the individual factors in order to characterise friction properly. To this end, computer simulations have been employed to complement experimental studies. The former techniques, chiefly molecular dynamics (MD), have in the past provided valuable mechanistic views on surface contacts[9–12] at the atomic scale.

Following our previous investigations of magnesium oxide (MgO) surfaces,[13] we use MD to investigate the contact behaviour of two more surfaces, sodium chloride (NaCl) and titanium dioxide (TiO_2). The former has a similar crystallographic structure (rock salt) to MgO and is therefore useful for making comparisons. The latter has a slightly more complicated crystallographic structure (rutile) and is an important industrial compound in the areas of catalysis and electrochemistry.[14]

Previously,[13] we investigated the commensurate contact behaviour between MgO probes of finite cross-sectional area with MgO surface slabs by monitoring the normal force, F_z, experienced by the rigid back-plane of the probe. Perhaps the most notable feature of the F_z *versus* d_z profile (where d_z is the distance between rigid planes of a probe and a slab) is the 'jump' process. This involved an abrupt and large change in F_z over a very short distance. Such features have also been observed in other studies involving tip–surface contact.[10,15] In this work, we found that NaCl systems also gave similar 'jump' features and that the 'jump' contact exponent was similar to that of MgO. However, TiO_2 systems gave more complex F_z *versus* d_z profiles, though the jump features were still observed. Bridging atoms were formed at the initial stage of the jump process. In the case of probe withdrawal, both NaCl and TiO_2 showed very different behaviour from the MgO, which showed a very systematic atom dislocation followed by probe elongation. In the case of NaCl, we observed complete probe withdrawal without any structural modification taking place, while TiO_2 showed a complex structural elongation.

Methodology

Model

The NaCl model is similar to that of MgO from our previous work.[13] The model consists of a slab of 16 × 16 rows of NaCl lattice (lattice parameter 2.789 Å) and 6 layers deep. Periodic boundary conditions were applied parallel to the surface (*x*–*y* directions) to mimic an infinite crystal surface. The surface slab was replicated in the *z* direction, with a vacuum gap of 66 Å between two surfaces in the resulting supercell. In order to simulate discrete (point-to-surface) contact, we have constructed NaCl blocks (probes) of finite cross-sectional area and 6 layers thick. Several $n \times n$ probes were constructed ($n = 2$, 4, 6, 8 and 10 atoms), effectively representing different degrees of surface roughness.

In the case of TiO_2, the most stable (110) surface contact was investigated. The (110) surface unit cell (1 × 1) has a dimension of $\sqrt{2}a \times c$ which, corresponds to 6.497 and 2.959 Å along the ($\bar{1}10$) and (001) directions, respectively. The surface contains five- and six-coordinate Ti^{4+} atoms and two types of O^{2-} atoms (in-plane and bridging). The six-coordinate cations are covered by the outermost bridging oxygen at the surface, while the five-coordinate cations are coordinated to in-plane oxygen atoms at the surface. We have constructed a (5 × 14) surface slab with a thickness of 15 atomic layers (containing 5 Ti–O layers). This corresponds to a dimension of 32.48 Å × 41.42 Å × 27.51 Å. Periodic boundary conditions were applied along the ($\bar{1}10$) and (001) directions of the surface, with a periodic vacuum gap of 65 Å in the direction normal to the (110) surface. Different probes were constructed as isolated blocks, using the Cerius^2 package,[16] with surface unit cells of ($2 \times m$), where m = 4, 5, 6, 7 and 8, replicated along the (001) direction. Each probe had a thickness of 19 atomic layers containing 6 Ti–O layers. Extra oxygen atoms were added to the top portions of the probes situated away from the surface slab. This was to maintain the overall neutrality of the systems. A typical initial set up of a TiO_2 system is shown in Fig. 1.

In both the NaCl and TiO_2 systems, probes were arranged to enable, respectively, (001) and (110) commensurate contact with the surface slab. The initial arrangement was such that each probe was placed near to the slab with a surface normal distance between the probe and the slab of 7 Å. At this distance, we have found that the slab–probe interactions are negligible. This distance was gradually reduced to simulate surface contacts by moving the probe in the *z* direction. The size of the slab ensured that interactions between probes of all sizes and their *x*–*y* periodic image counterparts were negligible at all times. For ease of description, we refer to the contact surfaces as active surfaces and the non-contact surfaces as base surfaces. For a probe, the base surface was held rigid, and can be regarded as the support base that attaches to an imaginary macroscopic body. We have not considered this body explicitly, as we assume that only the probe or protruding part of the imaginary body interacts with the surface slab significantly at any time. In fact, the distance between the base surface and active surface of a probe is about 3–4 Å longer than the cut-off distances set for the interatomic interactions. This means that there was no direct short range interaction between atoms from the rigid planes and those from active contacting surfaces.

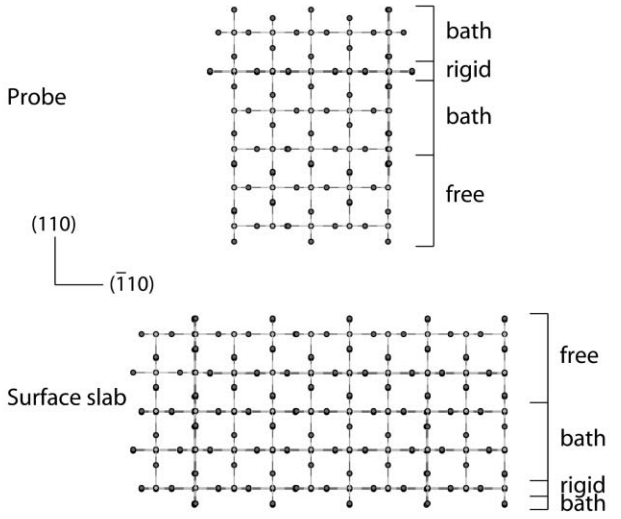

Fig. 1 Schematic representation of model of a ($2 \times m$) TiO_2 probe in commensurate contact with a (110) TiO_2 surface slab. The diagram indicates atom classifications as mentioned in the text. Probes of different sizes are replicated in the (001) direction (normal to the paper plane). Light spheres represent Ti and dark spheres represent O.

Previous work[17] shows that inclusion of mesoscopic interactions alters the quantitative results. However, the qualitative behaviour of the surface contact features are still largely preserved. In this work, we have not added additional bulk interactions between the probes and the surfaces. Instead, quantitative comparisons are only made between models of the same system, where a similar type of probe is used in all cases.

Molecular dynamics

We have used the DL_POLY[18] package to perform our MD simulations. The simulation approach we have used is similar to that in our previous work.[13] Basically, all atoms were classified into three different groups, depending on their initial positions: (a) atoms that are near and at the active surfaces where commensurate contacts would take place are allowed to move freely. (b) Atoms from the adjacent layers were coupled to the Berendsen heat bath[19] to maintain the temperature of the whole systems. (c) Atoms from the base surfaces were held fixed. The diagram for the assignment of atom types for the NaCl systems is similar to that of MgO, shown in Fig. 1 of our previous work.[13] In the case of TiO_2, it is shown in Fig. 1 of this paper. Note that the rigid base plane for a TiO_2 probe is the second most distant Ti–O plane from the active surface. Five atomic layers coupled to a Berendsen bath were added to the top of the rigid plane. Note that the use of the Berendsen bath for these additional layers of atoms may not be essential. The bath was simply introduced so that the rigid plane is sandwiched between atoms of equivalent type of trajectories. More importantly, the presence of these layers was found necessary to reduce strain artificially introduced by the atoms below the rigid plane as a result of natural dislocations at the probe. We shall come to this point later in the Results section. In this way, the time averaging for the F_z value was kept near to 0 nN, signifying negligible interaction between the active surfaces. We did not have a similar problem in the case of NaCl probes, which behaved like MgO.

All short range interactions were treated pairwise using Buckingham potentials, for which the parameters were obtained from Catlow *et. al.*[20] and Matsui and Akaogi[21] for NaCl and TiO_2, respectively. All atoms were treated as rigid ions, in preference to a breathable shell model,[22] for faster computation. We chose these potentials because they are found to reproduce features that are essential in surface contact studies, such as crystal structures and elastic constant values. In the case of TiO_2, the potential sets[21] are also able to reproduce structures and relative stabilities of the rutile, anatase and brookite phases of bulk TiO_2 that are in line with the experimental data. This suggests the force field is reliable over the whole range of crystalline polymorphs, a feature that may be essential when a TiO_2 probe is compressed against the surface at high pressure.

All the long range electrostatic interactions were evaluated by means of the 3D periodic Ewald summation, using the partial charge values of ± 0.988 for Na and Cl ions and +2.196

and −1.098 for the Ti and O ions, respectively. Previous detailed and systematic investigation of TiO_2 force fields found that formal charge rigid-ion models, in general, yield much larger values for elastic constants.[23] In other words, these models are all predicted to be too stiff. For this reason, and in addition to the reason mentioned above, we decided to use the partial charge model of ref. 21 for the TiO_2 systems.

Atomic trajectories were solved by the Verlet leap-frog algorithm[24] with a fixed time step of 0.5 fs. With the exception of fixed atoms, all atoms were assigned initial velocities with a Gaussian distribution equivalent to a temperature of 300 K. Systems were then allowed to equilibrate until a stable mean configurational energy was achieved. This usually took about 60–90 ps. In order to simulate body contacts, we employed similar procedures to those described in our previous work.[13] This involved movement of a probe by changing the position of its rigid plane by 0.5 Å along the z direction. After each movement, the whole system was allowed to equilibrate for 2000 time steps (1 ps) for NaCl and 1000 time steps (0.5 ps) for TiO_2. This was followed by data sampling and averaging over a further 1000 time steps for both systems. The choice of equilibration periods ensured that after each probe advancement step, the equilibration cycle was sufficiently long for the system to equilibrate before measurements were recorded. To obtain an F_z *versus* d_z profile of a system, the above-mentioned procedure was repeated so that the contact interaction over a whole range, from large d_z with no interaction to small d_z with large compression, was obtained. This procedure is equivalent to probe movement of 3.33 m s^{-1} for NaCl and 5 m s^{-1} for TiO_2.

Results

NaCl systems

(i) Incoming probes. The general features of the F_z profiles were rather similar to those of the MgO systems. However, F_z profiles for the NaCl systems were much noisier. This is not surprising, since NaCl has lower melting point (1074 K) and lattice energy compared with MgO, which has a high melting point of 3103 K. Consequently, lattice vibrations for NaCl crystals are larger and give rise to larger F_z fluctuations. For each NaCl probe, the most prominent feature was the characteristic 'jump' at a certain critical distance, d_z. For all NaCl probes, the magnitudes of the jumps were found to be much smaller than those of MgO, reflecting the lower cohesive energy of the NaCl crystal. Fig. 2 shows the F_z profiles for the incoming (6 × 6) and (10 × 10) NaCl probes. The behaviour of the other probes was entirely similar.

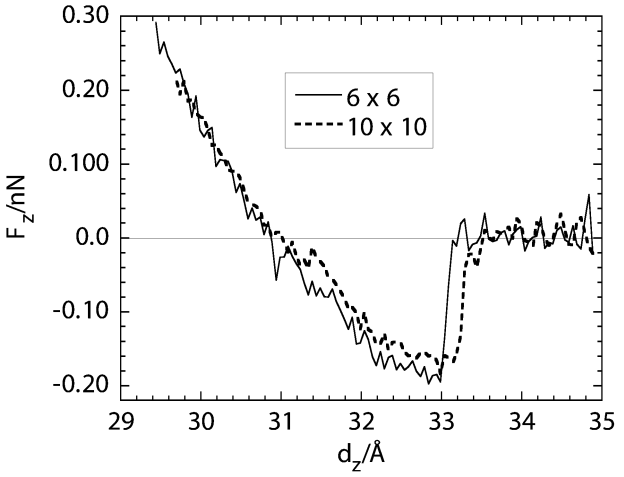

Fig. 2 F_z profiles of incoming (6 × 6) and (10 × 10) NaCl probes in commensurate contact with (001) surface slabs.

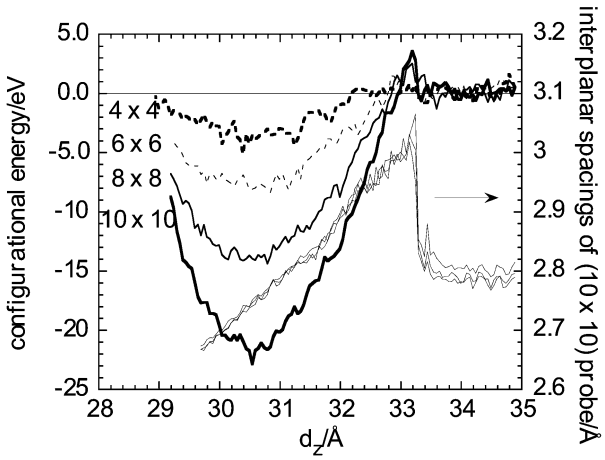

Fig. 3 Configurational energy profiles for NaCl probes. To aid comparisons, all energies are reset to the reference zero origin. The profiles of the first three interplanar spacings of the 10 × 10 probe that are nearest to the surface is also included, with the axis scale shown on the right.

There was a subtle difference between the NaCl and MgO profiles. In the latter case, a region of weak attraction was identified where there was a small gradual build up of F_z in the negative direction as d_z was decreased. At this stage, the probes were still essentially in an isolated stage, being located prior to the 'jump' process. However, no such region was identified for the NaCl systems. From Fig. 2, it can be seen that at large d_z the rigid plane of a probe experienced a net zero force, as expected. The situation persisted until the 'jump' process occurred, where attractive forces became sufficiently strong to bind the two bodies. This was also observed for all the other NaCl probes (not shown in Fig. 2).

At the jump process, the large change in F_z in the negative direction was simultaneous with a significant elongation of the probe as it was attracted towards the surface. This is illustrated in Fig. 3, which shows significant changes in the first three interplanar spacings for the (10 × 10) probe, which occurred at the distance d_z^j from the jump process ($d_z^j \approx 33.2$ Å). Interestingly, the elongation was also accompanied by a small increase in the configurational energy, as shown in Fig. 3. Such increases, however, became less apparent as the probe size decreased. This is in contrast to the incoming MgO probes, where no such energy barrier was observed. We note that since our systems were in equilibrium when measurements were taken, the presence of the energy barrier must be due to entropic effects, as can be demonstrated with the usual Helmholtz free energy expression

$$A = E - TS$$

Since contact between the probe and surface occurs as a spontaneous process (*i.e.* the force F_z is generally attractive—at least in the region in question), then any change in free energy A must be in the negative direction. If this occurs with an increase in system energy E, the contact process *must* occur with an increase in entropy S. That F_z is *not* the derivative of the system energy is clear from Fig. 4, which plots F_z and the configuration energy as a function of the z coordinate (the kinetic energy being constant at fixed temperature). However, the entropic contribution is evidently unimportant in the MgO systems. The F_z curves in that case clearly corresponded to the first derivative of the configurational energy, as was pointed out in our previous work.[13]

Beyond the jump region the force gradually increased and became positive as the probes compressed against the surface. Similar to the MgO systems, all NaCl probes, with the

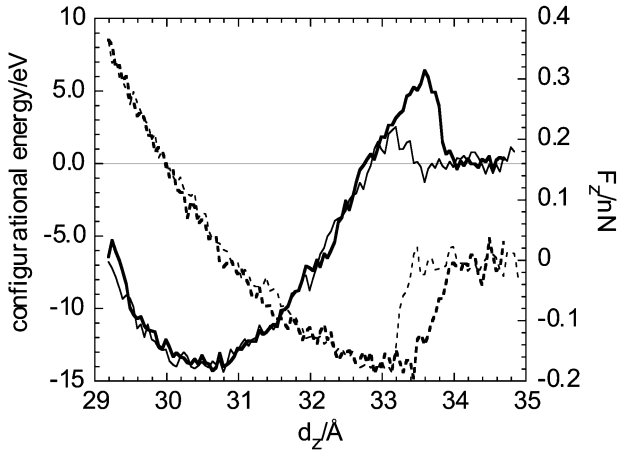

Fig. 4 Double plot showing the configurational energies, solid lines and the F_z profiles, dotted lines for the (8 × 8) NaCl probe. Bold curves indicate probe withdrawal. A horizontal line is drawn to indicate zero reference origin for the energy curves.

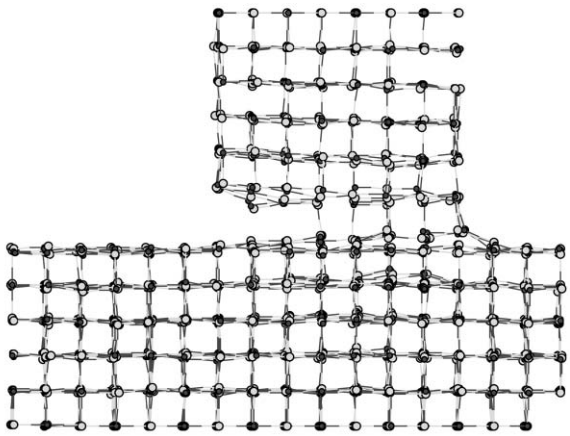

Fig. 5 Atomic configuration of the (8 × 8) NaCl probe withdrawal system that corresponds to the maximum energy at d_z = 33.6 Å.

exception of the smallest, displayed slight curvature in the repulsive region, signifying the compressions were not Hookian in nature. However, the F_z curves of the various MgO probes merged only at the most highly compressed state, whereas the merging occured at $F_z > 0$ nN for the NaCl probes, Fig. 2. This may reflect the relative softness of NaCl, in that the probe size is rather insensitive to compression.

(ii) Withdrawal of probes. Despite the similar crystallographic structures of NaCl and MgO, we found that a NaCl probe that was attached onto the surface could be lifted completely from the surface without permanent structural dislocation, nor deposition of probe fragments on the surface. This was observed for probes of all sizes. Such effects were not observed in the MgO systems where strong binding between the surface and probe resulted in irreversible systematic structural changes *via* a necking process.

Fig. 4 shows a double plot of F_z and configurational energy for the (8 × 8) NaCl probe initially moving towards the surface, followed by subsequent probe withdrawal. Up to distances less than d_z^j, the probe withdrawal was essentially reversible. That is, the F_z profiles for both incoming and outgoing probe followed the same path. However, hysteresis was clearly evident immediately after d_z^j, and the probe eventually separated from the surface completely. The corresponding energy profile for the withdrawing probe showed a much higher energy barrier over a larger distance than for the incoming process. An energy cost of about 6.4 eV was required to completely remove the probe from the surface.

Fig. 5 shows the configuration that corresponds to the maximum energy at d_z = 33.6 Å. The atoms are joined by connecting lines that can be used as a rough guide to visualise the extent of the expansion or compression of the system. (For example, a line is drawn between two atoms if the distance is close to the equilibrium value. However, no line is drawn between some of the adjacent Na and Cl pairs when distances exceed the equilibrium value.) It can be seen that the system is highly strained, especially at the surface–probe junction, where atoms from active surfaces were drawn towards one another and significantly away from their equilibrium positions. Some of the bonds have just been broken. This is apparent especially for atoms towards the left of the active surface of the probe, which were dislocated from their equilibrium positions. As the probe was further withdrawn from the surface, the remaining bonds at the surface–probe junction were subsequently broken and the atoms moved back to their original equilibrium positions. At this stage the probe was completely separated and the original equilibrium configuration was restored.

Visual inspection of the atomic configuration for the (10 × 10) NaCl probe withdrawal at the maximum configurational energy shows no qualitative difference from that Fig. 5. However, there were significant differences when comparing with Fig. 8(a) from our previous work.[13] In the latter case, the withdrawing (10 × 10) MgO was also located at the region of steep change in F_z. Three main differences were noted: (i) the strains were rather uniform throughout the NaCl probes. In the case of MgO probes, the initiation of neck formation was due to strain being localised near to the probe base, surface and at the centre. (ii) Atoms from the NaCl surface slab that were under a probe were significantly displaced from their original positions. The effect was observed even for atoms as deep as the third layer beneath the surface. In the case of MgO, such significant distortion was only apparent at the first layer. (iii) Bonds at the MgO probe–surface junction were systematically broken, starting from the corner edges of the probe. Conversely, no systematic trend could be clearly identified for the NaCl probes.

TiO_2 systems

(i) Incoming probes. Broadly speaking, the qualitative behaviour of TiO_2 contact interactions was similar to both NaCl and MgO systems, where the jump was still a characteristic feature of the F_z profiles for TiO_2 probes of various probe sizes, Fig. 6. Unlike the rock-salt systems, the magnitude of jump and position of occurrence in the TiO_2 systems were less sensitive to probe sizes. Furthermore, the force profiles show complex patterns at the region of high compression.

We have found that the potential selected for our TiO_2 system reproduced the usual (110) TiO_2 surface relaxation, with the interatomic distances comparable to those obtained from density functional calculations.[25] In the case of the probes, some restructuring around the outer layer was evident, although the overall structural integrity within the probe was still retained. As a result of the restructuring, a strain was found at the rigid planes of the probes which were fixed at the perfect crystallographic configuration. It was found necessary to add five additional atomic layers on top of the rigid plane so that the plane formed part of the bulk structure of the probe. In this way, an average zero F_z was registered on the rigid planes for probes situated far from the surface, signifying the strain on the rigid planes had almost been eliminated.

To highlight the detailed contact behaviour of TiO_2 systems, we present the (2 × 6) probe as an example. We note that the

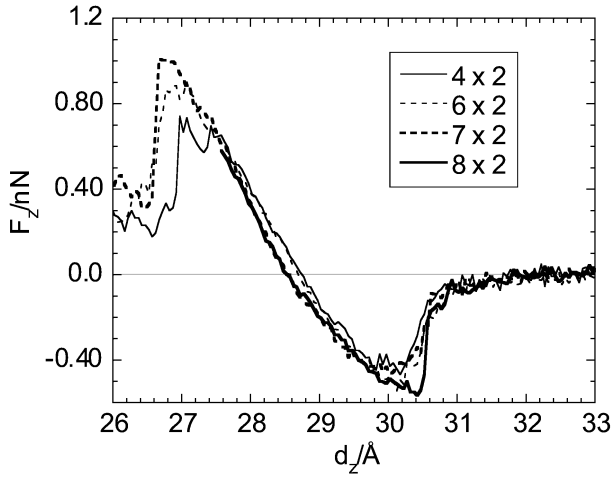

Fig. 6 F_z profiles of incoming TiO_2 probes in commensurate contact with the (110) surface slabs. The force profile for the (2 × 5) probe has been left out for clarity purposes.

same conclusions can be drawn for all other probes. In the early stages of contact is the region of gradually increasing F_z towards negative values at $d_z \approx 31$–32 Å, in which atoms from the probe began to realign to make commensurate contact with ions of opposite charges in the surface slab. Fig. 7 shows a series of snapshots of the (2 × 6) probe approaching the surface. The first visible sign of contact interaction was initiated *via* bridging of a few atoms between the surface and probe atoms. This marked the onset of a large negative increase in F_z. Fig. 7(a) shows one such configuration, near to the midpoint of the region. More bonds were gradually formed until the most negative value of F_z was obtained, which marked the end of the jump process, Fig. 7(b). The bond formations were progressive in nature as the ions at the probe realigned to make commensurate contact with the surface. This explains why the jump processes in the TiO_2 systems were generally not as abrupt as for the rock salt systems.

Noticeably, not all atoms from the probe's active surface were in direct commensurate contact with the surface when F_z was at a minimum, especially for those atoms at the edges of the probes, Fig. 7(b). Further compression resulted in gradual formation of bonds between these atoms and the surface counterparts, while the extended interplanar spacings decreased until the probe was almost contiguous with the surface slab, Fig. 7(c). At this stage the system was near to the most stable configuration (lowest configurational energy), with the rigid plane experiencing almost no vertical force. However some degree of atom dislocation was still evident around the outer layer of the probe. Moving the probe towards the surface beyond this point resulted in compression of the crystallographic structure and, thus, F_z increased in positive value. Unlike the rock-salt systems, the F_z curves for the TiO_2 systems were essentially linear at the repulsion region of $F_z > 0$ nN. This may be attributed to the different crystallographic structures of the systems. The more open TiO_2 structure allowed a more flexible response to compression when it was at a maximum. With $F_z = +0.85$ nN there was a major structural change, especially at the lower part of the probe, Fig. 7(d). The vertical interplanar O–Ti–O frame structures showed signs of puckering under the load. Further compressing the probe beyond this point led to the collapse of the internal structure, with more new bonds formed outside the perimeter of the probe, Fig. 7(e). Subsequently, a large drop in the value of F_z was registered. The onset of probe collapse apparently depends on probe size, as shown in Fig. 6. The larger the probe, the greater the load required at collapse, and subsequently the larger probes collapsed at a smaller value of d_z. Prior to the probe collapse, Fig. 7(d) shows a depression of the second atomic spacing, due to the compression of the probe. However, the depression was partially relieved when the probe collapsed.

In order to measure the structural integrity of the probes, we measured the density profiles along the (110) direction. Fig. 8 shows a series of density profiles that correspond to probes from Fig. 7. To facilitate comparison, the probes are repositioned so that the rigid planes in each configuration share a common horizontal coordinate. The most prominent peaks in each case corresponds to the rigid planes. For a perfect TiO_2 structure, two secondary peaks, which correspond to the two types of atomic layers containing oxygen ions, are sandwiched in between two primary peaks, which correspond to two similar atomic layers containing both Ti and O ions. Profiles corresponding to Fig. 7(a)–(c) indicate gradual restoration of probe structure towards the bulk rutile structure. The restructuring occurs throughout the jump process until $F_z \approx 0$ nN is reached. The density profile for Fig. 7(d) shows sign of peaks widening due to the puckering. Such effects are particularly severe towards the active surface of the probe. Finally, the density profile for Fig. 7(e) shows almost complete disorder at one end of the probe. It indicates that the structural disorder is rather extensive, involving almost the whole of the probe. Note that the structure of the first atomic layer that contains both Ti and O ions is preserved, due to constraints imposed by the rigid planes.

(ii) Withdrawal of probes. The withdrawal of TiO_2 probes in general showed far more complicated structural changes than both the MgO and NaCl systems. Once again, for illustrative purposes, we have confined our results to one probe, which in this case is the (2 × 5) TiO_2 probe. In Fig. 9, we present withdrawal of the (2 × 5) probe from several initial positions (in each case, the probe was withdrawn at the same rate as the incoming process). Four positions were selected, as indicated in Fig. 9: (a) $d_z = 30.42$ Å, the onset of the jump process or the region where a large increase in F_z over a small change in d_z occurs. (b) $d_z = 28.57$ Å, where $F_z \approx 0$ nN after the jump process has occurred. (c) $d_z = 26.97$ Å, the highly compressed state just before the probe collapses. (d) $d_z = 26.07$ Å, just after the probe has collapsed.

Probe withdrawals were almost always accompanied by hysteresis, with permanent structural changes to the probe but not to the surface. When pulling out the probe *during* the jump process, case (a), it was possible to withdraw the probe completely out of the surface with only minor structural changes to the active surface of the probe. The hysteresis is evident, with F_z showing a saw-tooth behaviour of decreasing magnitude towards 0 nN. From the atomic configurations, it was observed that this was a result of stepwise breaking of bridging bonds between the atoms from the surface and the probe. This was in contrast with MgO and NaCl probes where, prior to jump processes, the withdrawals were reversible and followed the same F_z curves to total probe–surface separation, with no change to the structure.

A probe withdrawn from any point after the jump process, but before the probe collapse, followed essentially the same path as the incoming process, see case (a), case (b) and case (c). However, hysteresis occurred when the probe was withdrawn from beyond the jump location. Evidently, the extent of hysteresis depends on the degree of probe compression.

During initial withdrawal, the structural changes were largely confined to the probe, with occurrence of the necking effect, except for those atoms from active surfaces which were essentially bound to the surface at this stage. Examination of the configurations revealed that formation of the 'neck' prior to elongation of the probe occurred at the lower part of the probe near to the contact junction. It involved a series of bond breakages leading to disruption of the crystallographic structure of this part of the probe. Fig. 10 shows a sequence of probe withdrawal process for case (b). Fig. 10(a) shows the

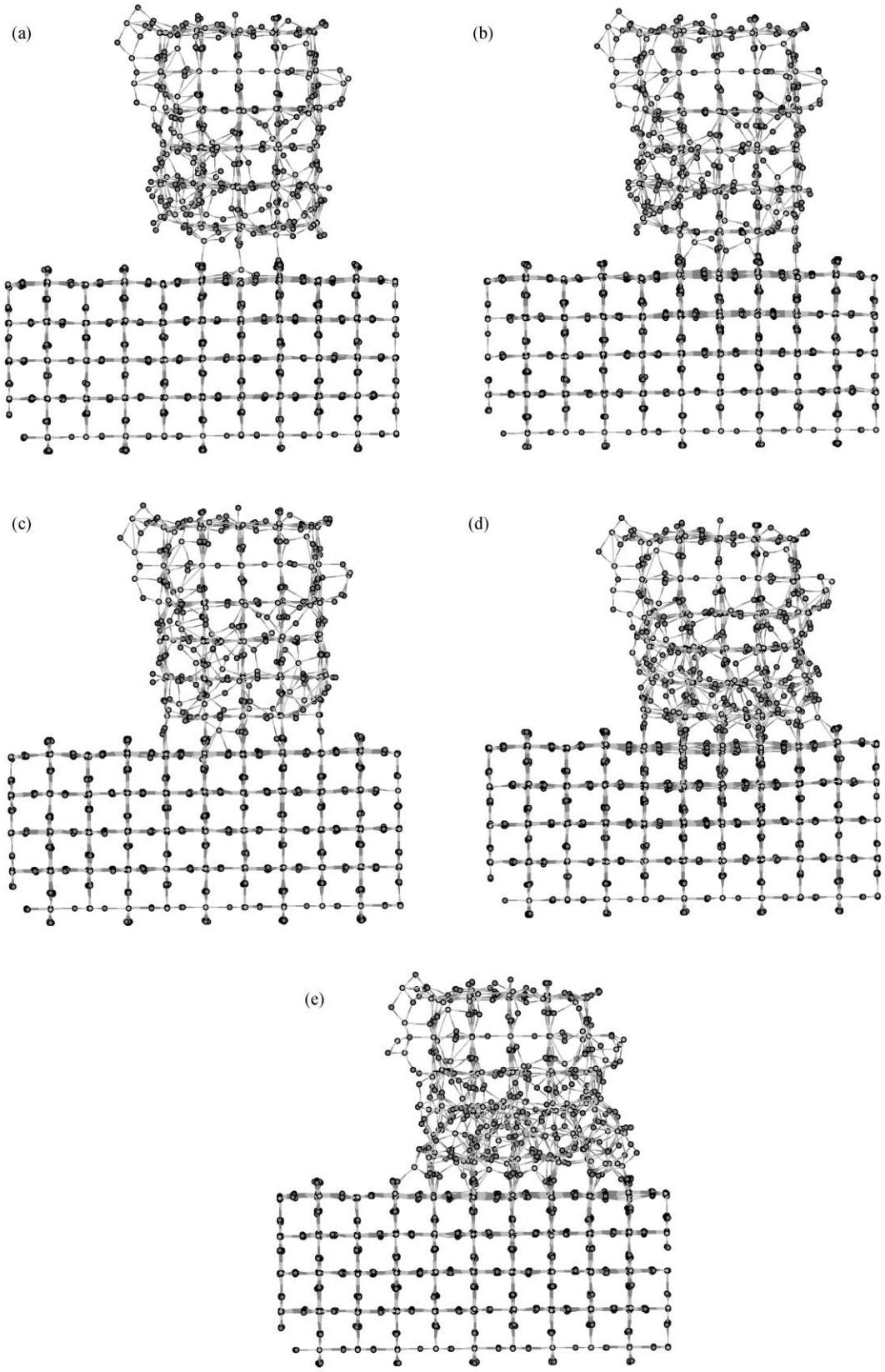

Fig. 7 Atomic configurations of incoming (2 × 6) TiO_2 probes. (a) d_z = 30.52 Å, F_z = −0.25 nN; (b) d_z = 30.12 Å, F_z = −0.54 nN; (c) d_z = 28.67 Å, $F_z \approx$ 0.0 nN; (d) d_z = 26.82 Å, F_z = +0.82 nN; (e) d_z = 26.17 Å, F_z = +0.25 nN.

highly stretched configuration which corresponds to the most negative value of F_z. Subsequent withdrawal of the probe over a small distance (∼0.5 Å) led to disruption of the crystal structure of the probe, forming a defect hole (marked with an asterisk), as shown in Fig. 10(b). The disruption involved a number of bond breakages in the vertical column of the Ti–O structure. This was registered as the first sharp increase in F_z and the sudden release of energy as the bonds broke.

As the probe was further withdrawn, the initial creation of the defect resulted in the formation of a neck, which elongated at the expense of further breaking of the vertical bonds, mostly in between the first two atomic planes that contained both Ti

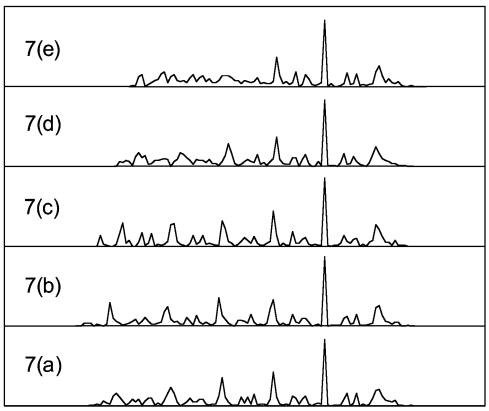

Fig. 8 Density profiles of (2 × 6) TiO_2 probes (excluding surface slab), along the (110) direction. The labels indicate the profiles that correspond to the atomic configurations of probes from Fig. 7.

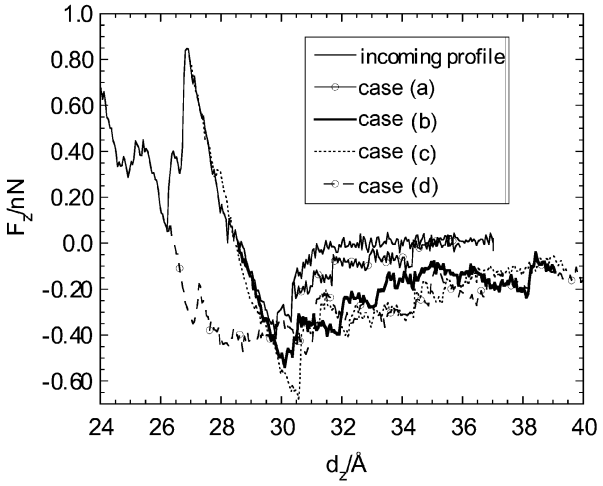

Fig. 9 F_z profiles of (2 × 5) TiO_2 probe withdrawal at different vertical distances: (a) d_z = 30.42 Å where the onset of the jump process occurs. (b) d_z = 28.57 Å, where $F_z \sim 0$ nN after the jump process has occurred. (c) d_z = 26.97 Å, which is at a highly compressed state, just before the probe collapses. (d) d_z = 26.07 Å, which is just after the probe has collapsed.

and O atoms. Bonds at the contact junction and the top part of the probe remained essentially intact. At a much later stage of withdrawal, only some of these bonds began to break. Fig. 10(c) shows the atomic configuration towards the end of our simulation (d_z = 41.6 Å). Notice that, even at this stage, the next three atomic planes that are nearest to the rigid plane are still visible, while most of the bonds are still intact at the contact junction.

Finally, for case (d), the withdrawal showed the greatest hysteresis effect. This was already clearly evident, even at the earliest stage of withdrawal, signifying that the collapse process was irreversible. Interestingly, Fig. 9 shows that the F_z profiles eventually became rather similar for all cases. This suggests a similar outcome would result at the final phase of the withdrawal. However, the exact nature of the final outcome to the withdrawal process—whether the probe would break, with some of its atoms left on the surface, or whether the probe would be totally withdrawn, with some materials from the surface attached to the probe—remains uncertain.

Discussion

Our results show that the jump process is a characteristic feature of the contact mechanisms for all the materials studied. While all of our results from this work, as well as those from the previous work and references therein,[13] show similar qualitative behaviour of F_z, the exact nature of contact and withdrawal of a probe depends not only on the crystal structures, but also on the nature of the crystal force. In the case of MgO and NaCl, which have similar crystallographic structures, the incoming contact behaviour is similar, but they show very different withdrawal behaviour. Specifically, the energy profiles of the NaCl systems show clear energy barriers for both the incoming process and the subsequent probe withdrawal. However, the withdrawal can be achieved completely without any structural change to the probe. Obviously, this discrepancy is largely due to the difference in the electrostatic interactions which are the dominant forces in ionic solids.

The occurrence of energy barriers when probes approach surfaces has been observed in contact studies of Lennard-Jones crystal surfaces.[26] The author suggested that such effects are entropic in nature, whereby the barriers coincide with the formation of bridging atoms, which provide an increase in entropy that outweighs the increase in potential energy. Our results also reveal the role of entropy. We confirm this conclusion from visual inspection of the graph from Fig. 4, which shows that the maximum configurational energy corresponds to the region of large increase of F_z in the negative direction, that is, *during* the occurrence of the jump process. The corresponding atomic configurations at this region show that only some commensurate 'bridging bonds' were formed, with the bonding atoms moved significantly out of the active surface plane. This distortion resulted in an increase in entropy. Complete bond formation occurred only at the minimum of the F_z profile. The return to an ordered structure resulted in decrease in entropy and, subsequently, the configurational energy also decreased.

The increase in entropy would be higher for large contact planes, since the surface distortions would be larger. This would occur with a higher configurational energy barrier, yet still reduce the free energy during a contact process. In addition, we have repeated a series of similar calculations on the NaCl systems at different temperatures and found that the energy barrier decreases as the temperature decreases. This observation is consistent with that of ref. 26. The differences in the contact mechanisms just described may have significant effects in the overall friction when two bodies slide. We will report our findings on these studies for both MgO and NaCl systems in future work.

The contact mechanisms for the TiO_2 systems are very different from the rock salt systems. In particular, the jump processes are less steep compared to the MgO and NaCl systems. This apparently depends on the degree of regularity of the contact surfaces. The contact process was initiated by the formation of a few bridging atoms at the junction. Note that the formation behaviour and the structure of the bridging atoms are less well ordered when compared with that of NaCl mentioned above. In fact, our observations are rather similar to the Lennard-Jones systems investigated in other work,[27] whereby bridges were initially formed prior to a collapse (avalanche) of surfaces. As the temperature increases, an avalanche is initiated by the formation of bridges at large separations, with the formation of defects such as vacancies and dislocations at the surface, and also in the bulk.[27]

In our case, the formation of bridges is mostly commensurate in nature, which reduces surface defects. This implies the presence of a much more ordered surface slab that helps to match the lattice with the probe surface. Such 'surface-healing' processes may explain the relative steepness of the F_z profiles during the jump process. Indeed, Fig. 6 shows that the steepness, in general, increases as the size of the probe increases. This is reasonable, since the larger the probe, the easier it is to retain the regular structure of the surface and,

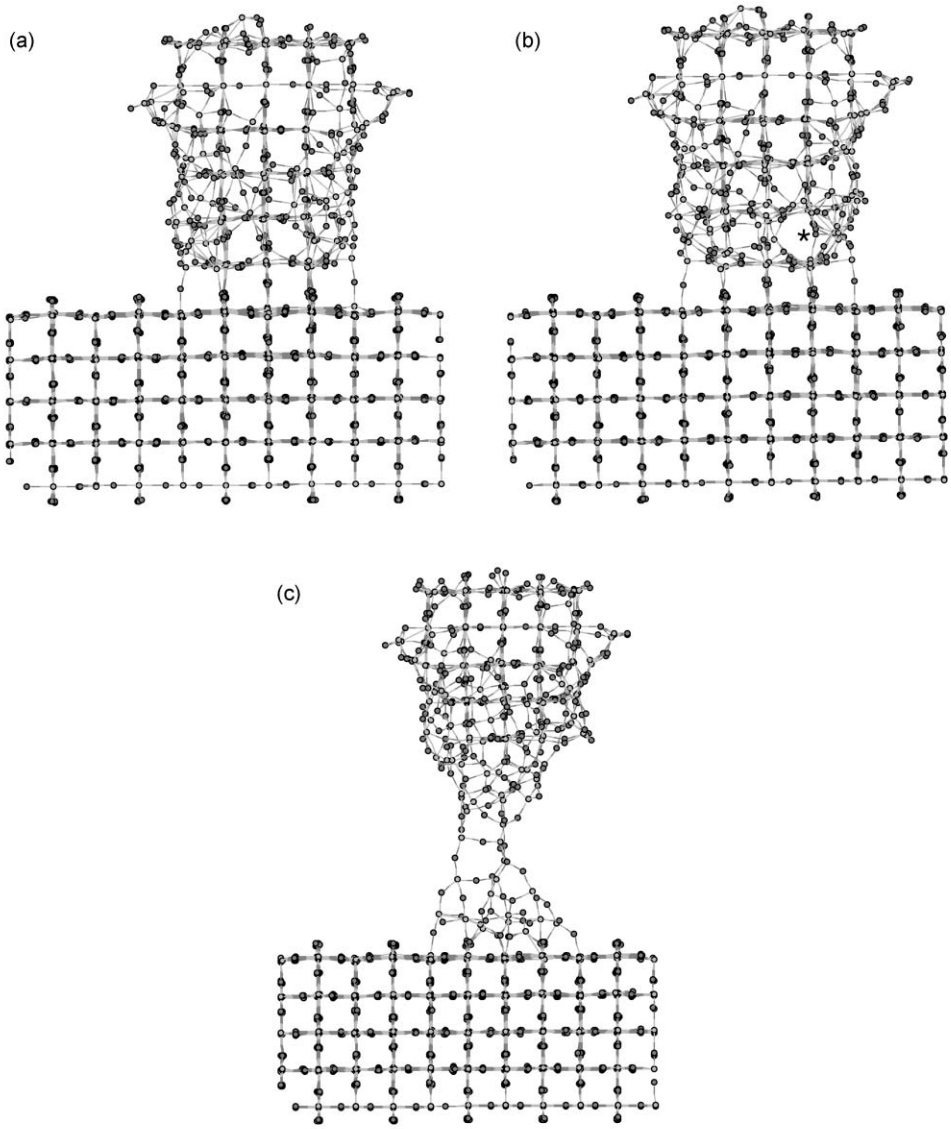

Fig. 10 Atomic configuration for the (2 × 5) TiO_2 probe withdrawn from $d_z = 28.57$ Å [corresponding to case (b) in Fig. 9]. (a) The probe is highly stretched at minimum F_z, where $d_z = 30.1$ Å. (b) Disruption to the crystallographic frames of the probe, marked with an asterisk, at $d_z = 30.6$ Å. (c) The configuration towards the end of the simulation at $d_z = 41.6$ Å.

hence, less reorganisation of the atoms would be required during surface contacts. Other work involving the fusion of two TiO_2 nanoclusters[28] revealed that contacts took place *via* initial surface distortion and some bridges were also visually evident in their figures. The overall contacts also occurred without fracture or elastic rebound. Such observations are in agreement with our work.

In Fig. 11 we find that the area of contact of TiO_2 is proportional to total load, derived from the minimum F_z multiply by the number of rigid atoms at the probe. This observation is in agreement with the theory of friction[29] which indicates that where only the apexes of asperities touch, the actual area of contact is proportional to load. Note that there is a considerable spread of the data in Fig. 11 and the straight line is derived from a least square fit with a correlation coefficient of 0.96. The main assumption of the result is that contact areas are equal to the surface unit cells of the probes. In reality, the apparent contact area of a probe is not well defined, due to the inherent structural disorder at the active surface. A similar graph was plotted for the MgO systems in our previous work,[13] which gives a clearer linear relationship due to the more well-defined apparent contact area of the rigid structure.

However, the conclusion we can arrive at is that while frictional contact is dependent on the load and the apparent microscopic contact area, it is independent of the nature and structure of the surface contact. For the latter case, it could be

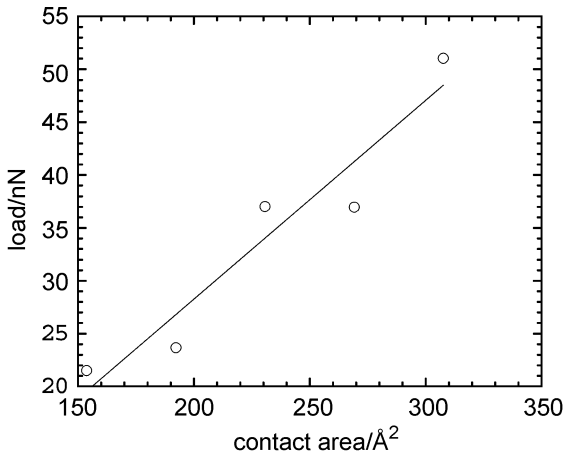

Fig. 11 Total load at the rigid plane of probes at minimum F_z *versus* contact area, estimated from the area of the rigid plane of the probes.

an atomically smooth block, such as MgO, or a block with structural defects, such as TiO_2, or even atomically sharp apexes. The jump process is the prominent characteristic feature of body contacts and also may be a fundamental component of friction. Therefore, it would be interesting to relate jump processes to the standard frictional laws which are commonly upheld for many materials.

Hysteresis always occurred when a TiO_2 probe was withdrawn from any distance after a contact had occurred. There is some evidence, though not conclusive, that the greater the load, the greater the extent of the resulting hysteresis. Such a dependence was not observed in the rock salt systems. The discrepancy may be due to the relatively open crystal structure of TiO_2 that is easier to collapse when compared with the close-packed rock salt structures. Other work involving contact studies of softer materials like surfactant monolayers[30] shows that frictional forces are dependent upon the extent of hysteresis, which in turn depends on the extent of interpenetration across the contact junction.

In our case, the extent of penetration of solid surfaces by the probes is negligible. However, significant probe deformation results as it is pressed against the surface. If the applied load is large enough, it eventually leads to fusion at the contact junction, with extra bonds formed outside the perimeter of an undeformed probe. Obviously, more force would be required to break these extra bonds if the collapsed probe is to be pulled apart. We have estimated that for the smallest probe, (2×4), to collapse would require a pressure of about 21.9 GPa, a magnitude that may not be achieved for free powder flows under normal circumstances. Nevertheless, in reality, the extent of surface asperity may well be much smaller than the smallest probe we have considered and, hence, may fuse at a much smaller load.

We have also noticed that when withdrawing TiO_2 probes, the formation of a neck is initiated by the creation of defects in the probe. This is also the case for the MgO systems obtained in our previous studies[13] and also from other studies involving breaking of gold nanowires.[31] The mechanisms of defect formation differ from one material to another. In the case of TiO_2, the defect apparently initiated at the relatively weak part of the crystal structure containing the 3-coordinate oxygen atomic planes. In particular, the bonds that are singly coordinated to Ti atoms and aligned along the direction of withdrawal are particularly prone to breakage when a probe is withdrawn from the surface. This suggests that the initial creation of defects is dependent on the withdrawal direction and the surface from which a material is withdrawn.

Summary

We have used molecular dynamics simulations to study in detail the contact behaviour of NaCl and TiO_2 and then make comparisons with that of MgO from our previous work. We have found that the 'jump' process is a common behaviour of contact mechanisms and may be universal. Nevertheless, the detailed nature of the 'jump' may be dependent on several factors, such as crystal forces, the underlying bulk crystal structures and the structures of the contact surfaces. Furthermore, the question of the relevance of the jump processes to the origin of friction has been raised. Chiefly, the processes have a simple linear relation with the apparent area of contact. Such a relationship does not depend on the nature and structure of the contact surfaces. In addition, we have also identified the possibility that the extent of hysteresis relates to the frictional force in TiO_2. The hysteresis relates to the way a probe is compressed. Previous work that was based on soft materials has also identified such a possibility, but related the hysteresis to the extent of penetration and the structure of the molecules across the contact junction.

Acknowledgements

This research was carried out under a research grant from the EPSRC. The simulations were performed on the Daresbury Laboratory IBM SP/2 computer. We are grateful to L. V. Woodcock for helpful discussions. We also wish to thank one of the referees, who brought ref. 17 to our attention.

References

1 D. Dowson, *History of Tribology*, Longman, London, 1979.
2 P. A. Cundall and O. D. L. Strack, *Geotechnique*, 1979, **29**, 47.
3 D. Hirshfeld and D. C. Rapaport, *Phys. Rev. E*, 1997, **56**, 2012.
4 J. Baxter, U. Tüzün and J. Burnell, *Phys. Rev. E*, 1997, **55**, 3546.
5 G. Binnig, C. F. Quate and Ch. Gerber, *Phys. Rev. Lett.*, 1986, **56**, 930.
6 C. M. Mate, G. M. McClelland, R. Erlandsson and S. Chiang, *Phys. Rev. Lett.*, 1987, **59**, 1942.
7 O. Marti, J. Colchero and J. Mlynek, *Nanotechnology*, 1990, **1**, 141.
8 M. Hirano, K. Shinjo, R. Kaneko and Y. Murata, *Phys. Rev. Lett.*, 1997, **78**, 1448.
9 J. A. Harrison, D. W. Brenner, C. T. White and R. J. Colton, *Thin Solid Films*, 1991, **206**, 213.
10 U. Landman, W. D. Luedtke and E. M. Ringer, *Fundamentals of Friction: Macroscopic and Microscopic Processes*, ed. I. L. Singer and H. M. Pollock, Kluwer, Dordrecht, 1992, p. 463 and references therein.
11 J. A. Harrison, C. T. White, R. J. Colton and D. W. Brenner, *Phys. Rev. B*, 1992, **46**, 9700.
12 K. J. Tupper and D. W. Brenner, *Thin Solid Films*, 1994, **253**, 185.
13 C. W. Yong, W. Smith and K. Kendall, *J. Mater. Chem.*, 2002, **12**, 593.
14 S. Semancik and R. E. Cavuchi, *Appl. Surf. Sci.*, 1993, **70/71**, 337.
15 A. L. Shluger, A. L. Rohl, D. H. Gay and R. T. Williams, *J. Phys. C*, 1994, **6**, 1825.
16 Cerius^2, Molecular Simulations Inc., San Diego, CA, USA, 1997.
17 A. L. Shluger, A. L. Rohl, R. T. Williams and R. M. Wilson, *Phys. Rev. B*, 1995, **52**, 11398.
18 W. Smith and T. R. Forester, DL_POLY, version 2.12, CCLRC, Daresbury Laboratory, UK, 2001.
19 H. J. C. Berendsen, J. P. M. Postma, W. F. van Gunsteren, A. DiNola and J. R. Haak, *J. Chem. Phys.*, 1981, **81**, 3684.
20 C. R. A. Catlow, K. M. Diller and M. J. Norgett, *J. Phys. C.*, 1977, **10**, 1395.
21 M. Matsui and M. Akaogi, *Mol. Simul.*, 1991, **6**, 238.
22 B. G. Dick and A. W. Overhauser, *Phys. Rev.*, 1958, **112**, 90.
23 D. R. Collins and W. Smith, *Evaluation of TiO_2 Force Fields*, CCLRC Technical Report DL-TR-96-001, Daresbury Laboratory, UK, 1996.
24 A. R. Leach, *Molecular Modelling: Principles and Applications*, Longman, Singapore, 1996.
25 S. P. Bates, M. J. Gillan and G. Kresse, *J. Phys. Chem. B*, 1998, **102**, 2017.
26 R. M. Lynden-Bell, *Surf. Sci.*, 1991, **224**, 266.
27 M. Lupkowski and J. F. Maguire, *Phys. Rev. B*, 1992, **45**, 13733.
28 D. R. Collins, W. Smith, N. M. Harrison and T. R. Forester, *J. Mater. Chem.*, 1997, **7**, 2543.
29 J. A. Greenwood, *Trans. ASME*, 1967, **89**, 81.
30 H. Yoshizawa, Y-L. Chen and J. Israelachvili, *J. Phys. Chem.*, 1993, **97**, 4128.
31 E. Z. da Silva, A. R. J. da Silva and A. Fazzio, *Phys. Rev. Lett.*, 2001, **87**, 256102.